Supporting Information

A simple and efficient Fluorophoric probe for dual sensing of Fe^{3+} and F^-: Application to bioimaging in native cellular iron pool and live cell

Chirantan Kar[a], Soham Samanta[a], Sandipan Mukherjee[b], Barun K. Dutta[a], Aiyagari Ramesh[b] and Gopal Das*[a]*

[a] Department of Chemistry, Indian Institute of Technology Guwahati, Assam, 781 039, India.

[b] Department of Biotechnology, Indian Institute of Technology Guwahati, Assam, 781 039, India.

E-mail: gdas@iitg.ernet.in; aramesh@iitg.ernet.in

Fax: +91-361-258-2349; Tel: +91-361-258-2313

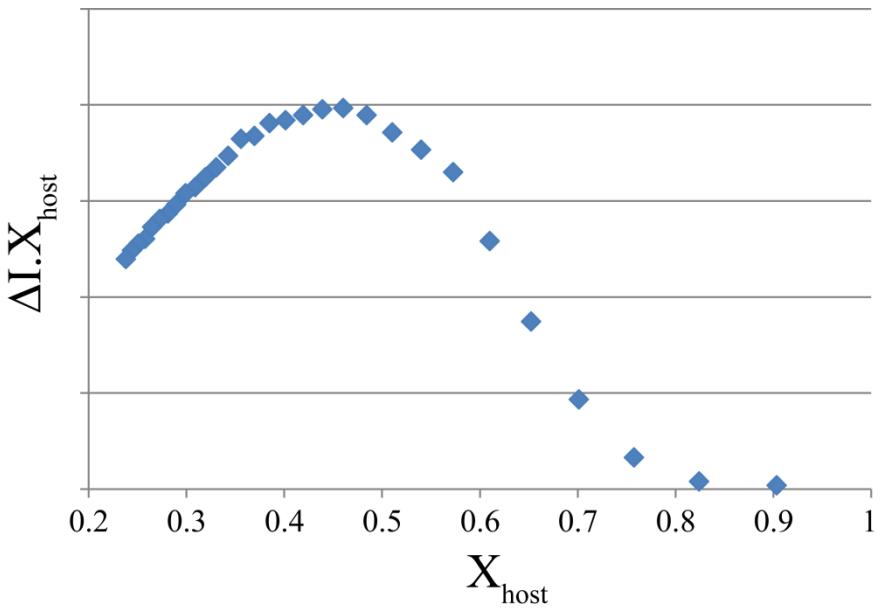

Figure S1: Job's plot between $\mathbf{L_1}$ and Fe^{3+} ions. Where X_{host} = the mole fraction of $\mathbf{L_1}$ and ΔI is the change $(I-I_0)$ in the intensity of the emission spectra in presence of guest.

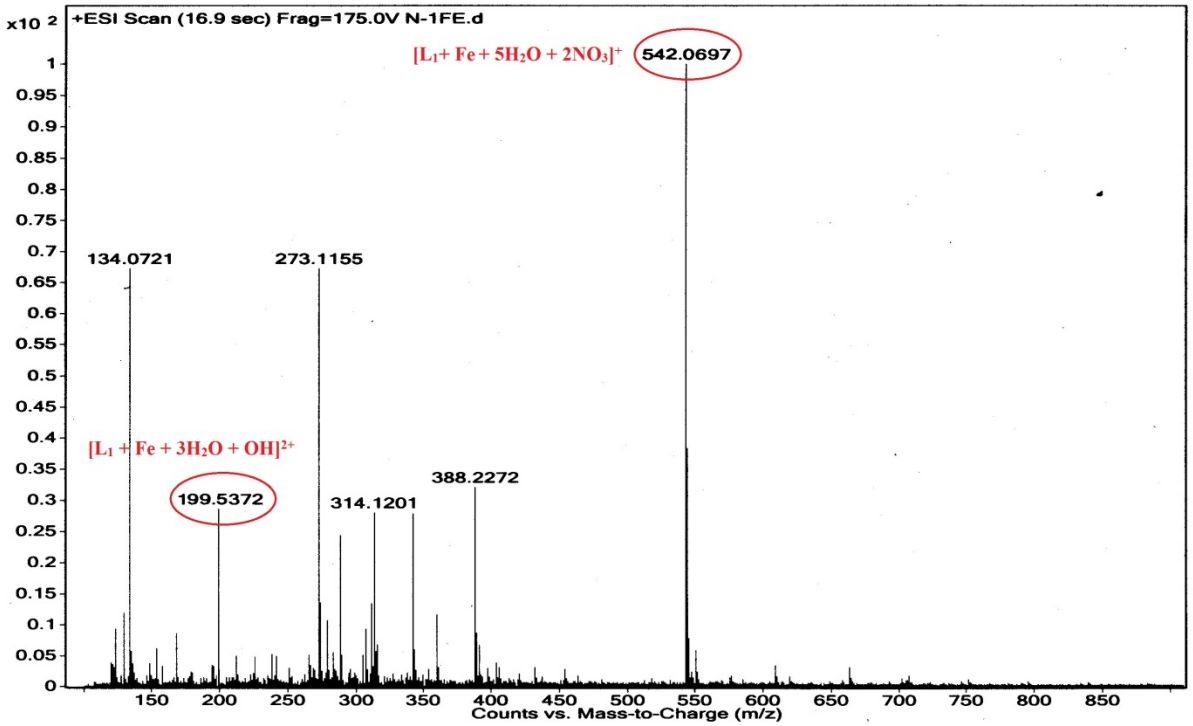

Figure S2: Mass spectrum of $\mathbf{L_1}$-Fe complex.

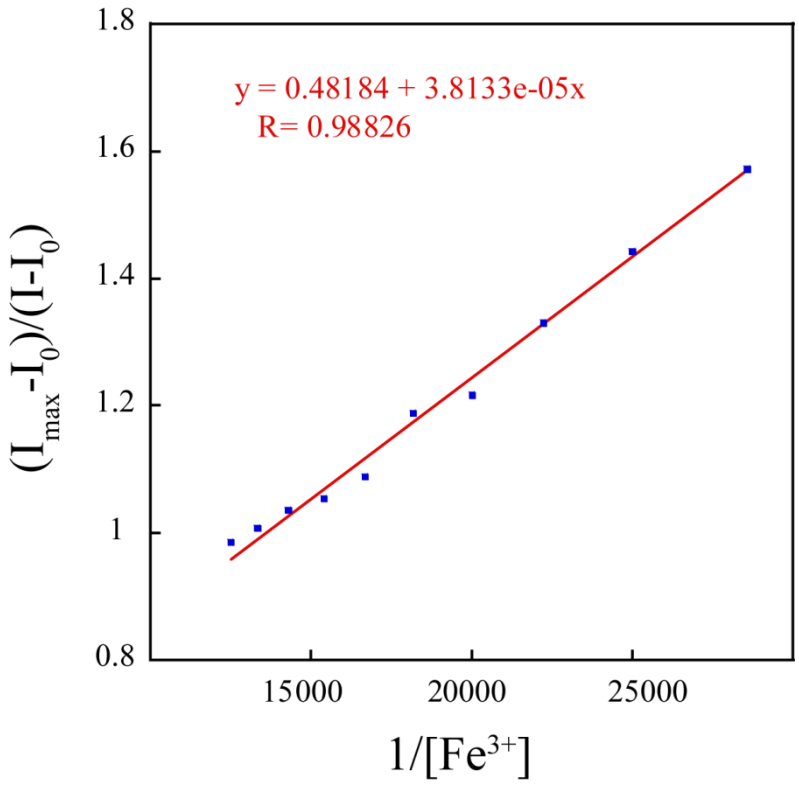

Figure S3: Bensei-Hildebrand plot obtained from the fluorescence emission (calculated at λ_{em}) studies.

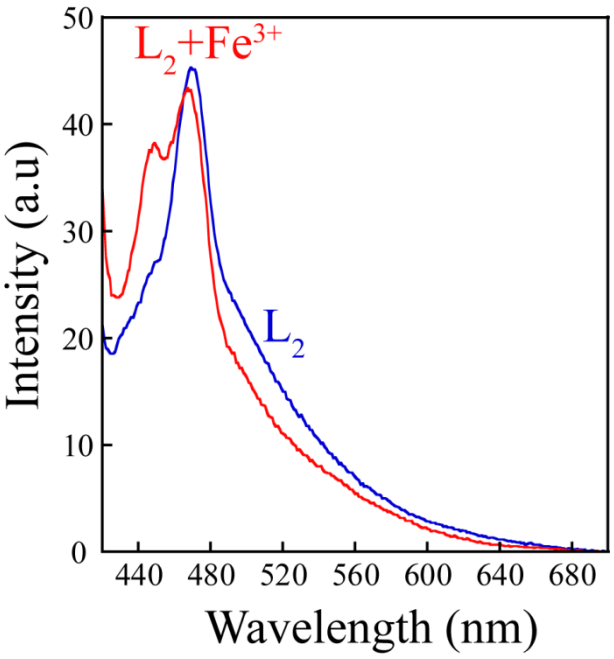

Figure S4: Changes of the of fluorescence emission of compound $\mathbf{L_2}$ (10 μM) observed upon addition of 10 eqv. of Fe^{3+} ions.

Occupied Orbitals	Energy (eV)	Vacant Orbitals	Energy (eV)
HOMO -2 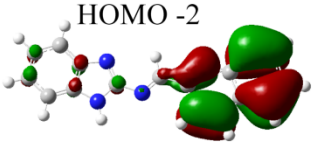	-6.5079	LUMO 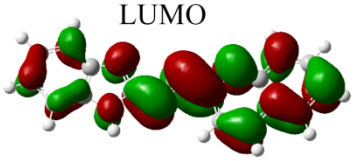	-2.2675
HOMO -1 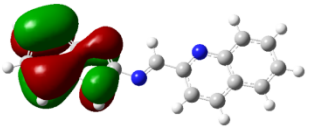	-6.1375	LUMO+1 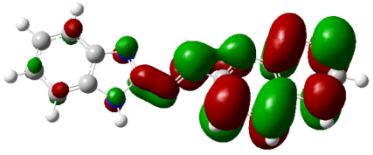	-1.2215
HOMO 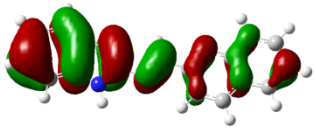	-5.7351	LUMO+2 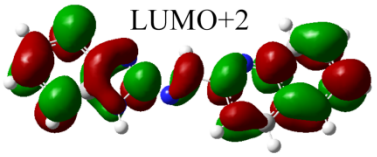	-0.1913

Figure S5: Selected orbitals and their energies for $\mathbf{L_1}$ at B3LYP/6-31G(d).

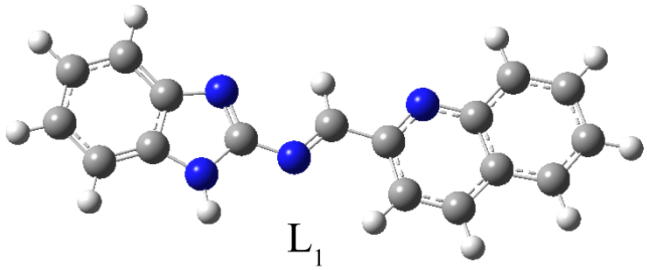

L_1

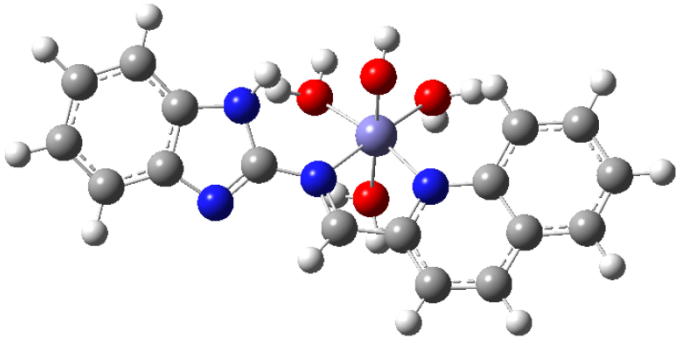

$[Fe\ (L_1)(H_2O)_3(OH)]^{2+}$

Figure S6: Optimized proposed structures of $\mathbf{L_1}$ and $\mathbf{L_1}$**-Fe** complex

Center	Atomic	Atomic	Coordinates	(Angstroms)	
Number	Number	Type	X	Y	Z

1	6	0	-3.94656	0.720773	-4.1E-05
2	6	0	-4.26671	-0.66523	0.000053
3	6	0	-5.58285	-1.13174	0.00014
4	6	0	-6.5881	-0.16937	0.000128
5	6	0	-6.29064	1.209949	0.000036
6	6	0	-4.97959	1.669673	-4.6E-05
7	6	0	-2.0726	-0.3138	-8.3E-05
8	1	0	-5.81569	-2.19214	0.000212
9	1	0	-7.62619	-0.48772	0.000194
10	1	0	-7.10828	1.924401	0.000029
11	1	0	-4.7455	2.729038	-0.00013
12	6	0	0.163272	0.188487	-0.0001
13	1	0	-0.06494	1.257634	-0.00014
14	6	0	1.587802	-0.16135	-6.5E-05
15	6	0	2.016518	-1.52101	-7.5E-05
16	6	0	3.76025	0.615636	0.000009
17	6	0	3.359969	-1.78914	-4.2E-05
18	1	0	1.267398	-2.30379	-0.00011
19	6	0	4.659107	1.716218	0.000063
20	6	0	4.290985	-0.71599	0.000003
21	1	0	3.726522	-2.8126	-4.2E-05
22	6	0	6.018967	1.504142	0.000097
23	1	0	4.233042	2.713918	0.000069
24	6	0	5.696156	-0.90023	0.000038
25	6	0	6.542237	0.187224	0.000083
26	1	0	6.70068	2.349384	0.000132
27	1	0	6.094457	-1.9115	0.000031
28	1	0	7.61787	0.038469	0.000111
29	7	0	2.423765	0.87028	-2.1E-05
30	7	0	-0.75155	-0.71853	-9.6E-05
31	7	0	-2.57876	0.904484	-0.00013
32	7	0	-3.04233	-1.29691	0.000017
33	1	0	-2.8465	-2.28576	0.000079

Rotational constants (GHZ): 1.505329 0.101277 0.094893

Figure S7: Coordinates for optimized geometry of $\mathbf{L_1}$ at B3LYP/6-31G(d,p).

Center	Atomic	Atomic	Coordinates	(Angstroms)	
Number	Number	Type	X	Y	Z

1	6	0	-4.15873	0.96518	0.058624
2	6	0	-4.04387	-0.2774	-0.62417
3	6	0	-5.14743	-0.95835	-1.12573
4	6	0	-6.38741	-0.35979	-0.90749
5	6	0	-6.52185	0.864597	-0.21098
6	6	0	-5.41918	1.54183	0.284585
7	6	0	-2.06922	0.548694	-0.0468
8	1	0	-5.06158	-1.89875	-1.65914
9	1	0	-7.28006	-0.85098	-1.28042
10	1	0	-7.51399	1.279179	-0.06941
11	1	0	-5.50995	2.483883	0.812994
12	6	0	-0.05761	1.74934	0.110683
13	1	0	-0.59263	2.695979	0.089735
14	6	0	1.384047	1.66554	0.110088
15	6	0	2.233869	2.785824	0.172073
16	6	0	3.176221	0.203706	-0.34455
17	6	0	3.594758	2.588729	0.053589
18	1	0	1.812779	3.774741	0.315311
19	6	0	3.646756	-1.04959	-0.81591
20	6	0	4.102871	1.300644	-0.23385
21	1	0	4.280507	3.426766	0.134536
22	6	0	4.990783	-1.22873	-1.07129
23	1	0	2.925221	-1.8003	-1.12181
24	6	0	5.482954	1.063142	-0.47188
25	6	0	5.922759	-0.18125	-0.86094
26	1	0	5.339208	-2.17593	-1.47089
27	1	0	6.179902	1.888831	-0.36782
28	1	0	6.976091	-0.354	-1.05275
29	7	0	1.853277	0.400553	-0.05177
30	7	0	-2.90799	1.44249	0.403666
31	1	0	-1.87089	-1.84777	0.677163
32	26	0	0.475353	-0.91925	0.375109
33	7	0	-0.69042	0.608062	0.051899
34	8	0	-1.01151	-2.05733	1.112838
35	1	0	-0.91034	-3.02223	1.139648
36	8	0	0.614449	-0.39574	2.390773
37	1	0	0.92487	0.462841	2.717628
38	1	0	-0.17004	-0.6339	2.911741
39	8	0	1.634875	-2.45562	0.987627
40	1	0	2.510655	-2.55784	0.574844
41	1	0	1.791403	-2.43868	1.946752
42	8	0	0.286139	-1.51757	-1.27376
43	1	0	0.351014	-2.48657	-1.32608
44	7	0	-2.66958	-0.58337	-0.62034
45	1	0	-2.2084	-1.04158	-1.40522

Rotational constants (GHZ): 0.490834 0.103481 0.094098

Figure S8: Coordinates for optimized geometry of $\mathbf{L_1}$ at B3LYP/6-31G(d,p)

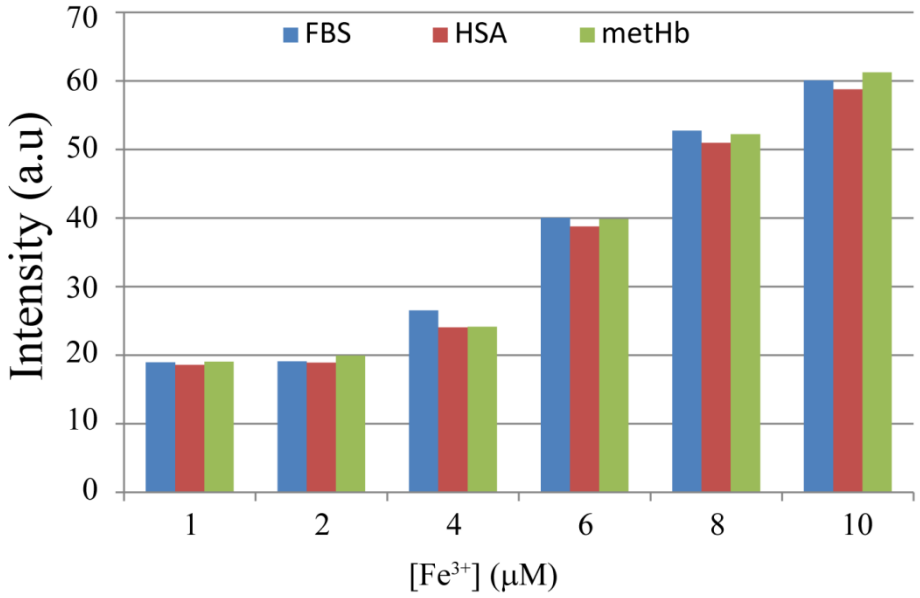

Figure S9: fluorescence emission (calculated at λ_{em}) of $\mathbf{L_1}$ on addition of increasing concentration of Fe^{3+} in different protein environment.

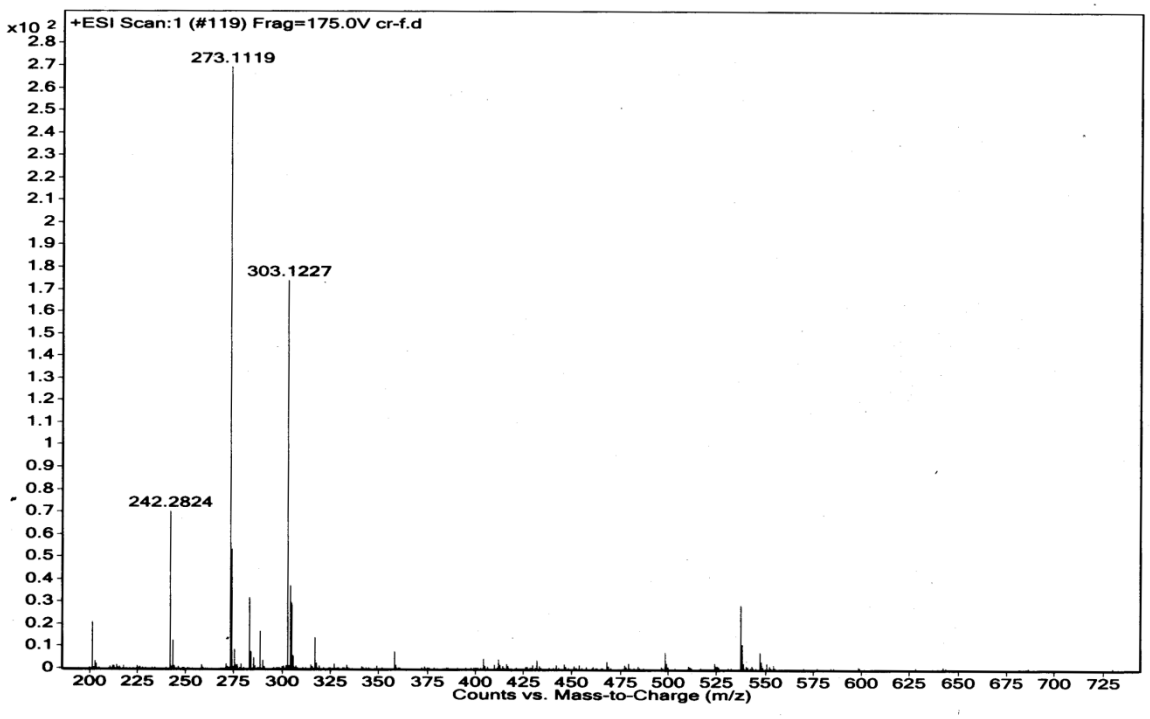

Figure S10: Mass spectrum of $\mathbf{L_1}$-**Fe**+Fluoride

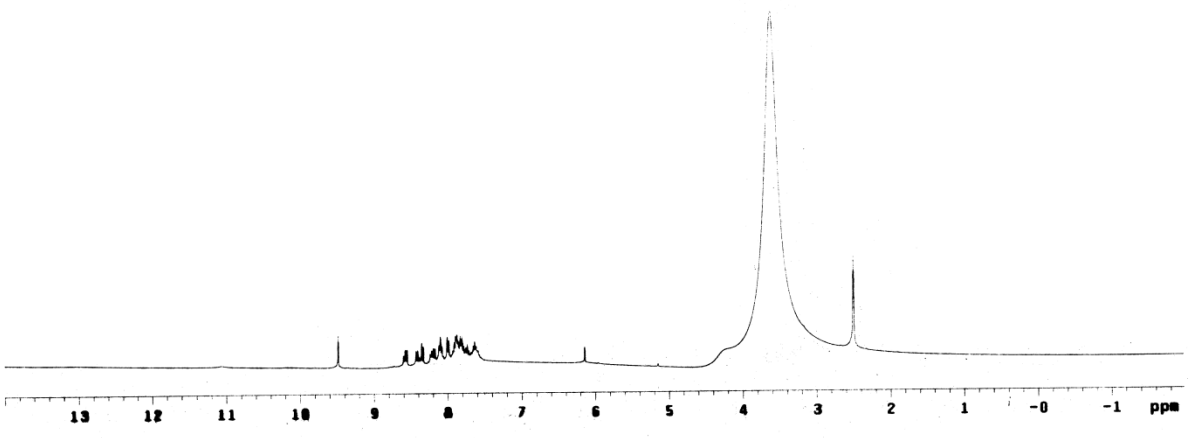

Figure S11: ^{1}H NMR spectrum of $\mathbf{L_1}$ in DMSO-d_6 solution.

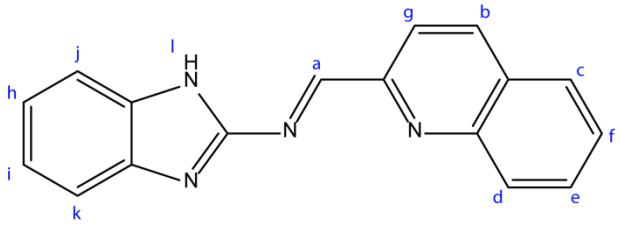

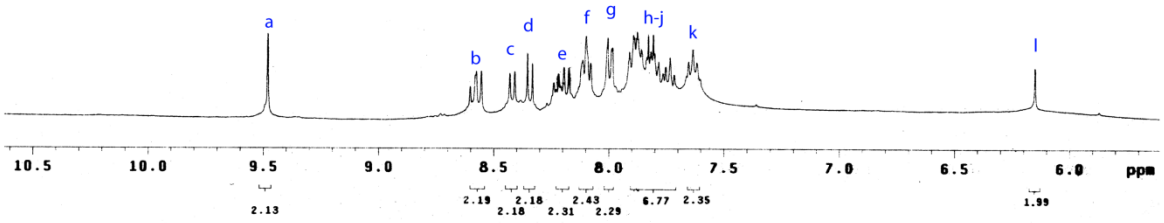

Figure S12: ^{1}H NMR spectrum of $\mathbf{L_1}$ in DMSO-d_6 solution (expanded aromatic part).

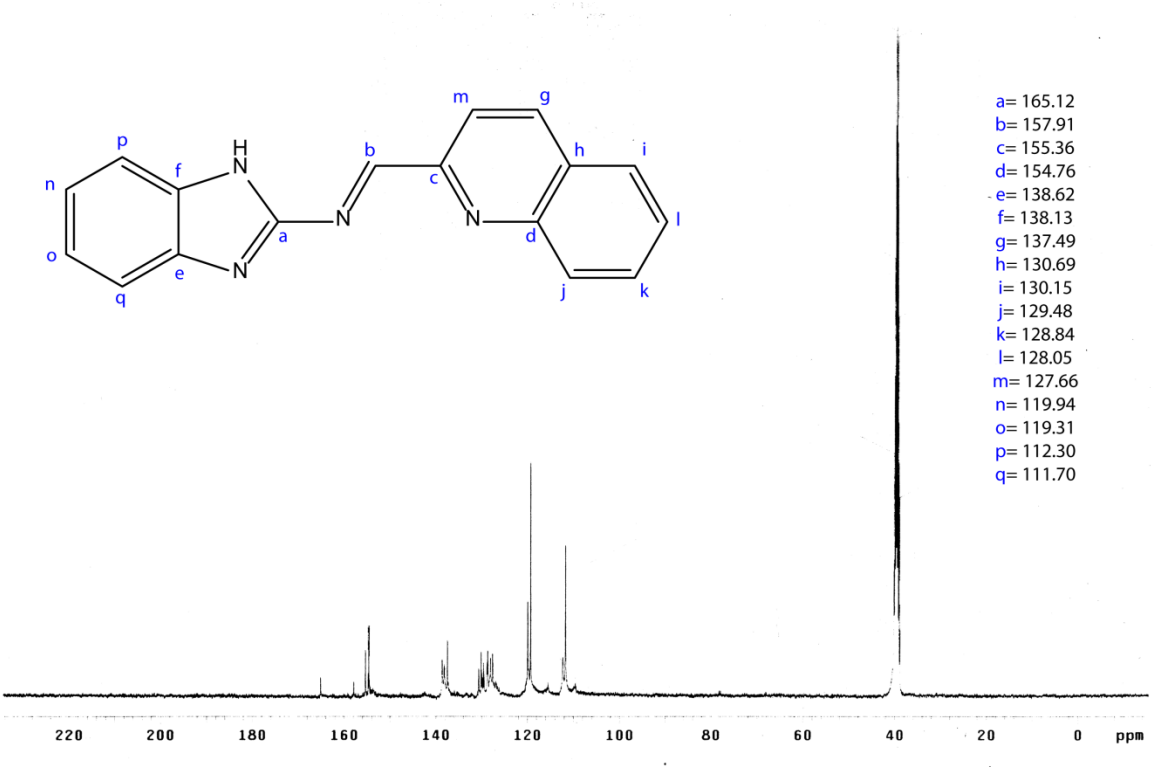

Figure S13: ^{13}C NMR spectrum of $\mathbf{L_1}$ in DMSO-d_6 solution.

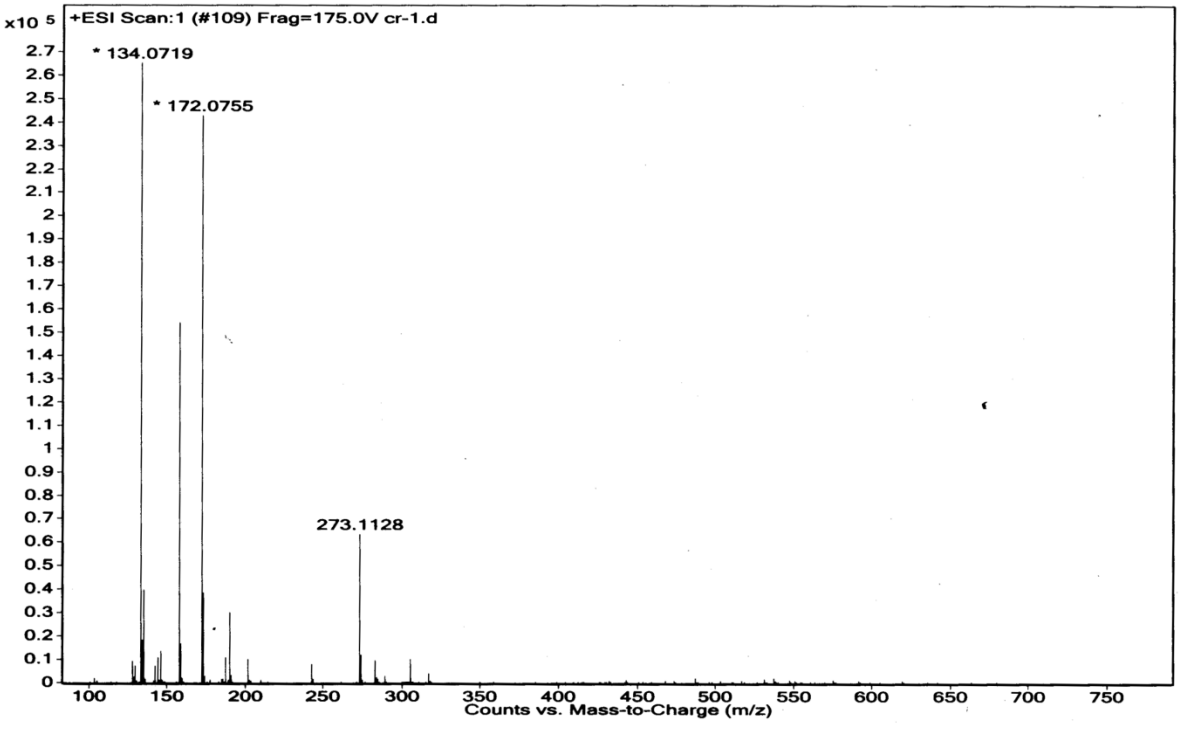

Figure S14: Mass spectrum of $\mathbf{L_1}$ (Mass spectrum obtained in positive mode)**.**

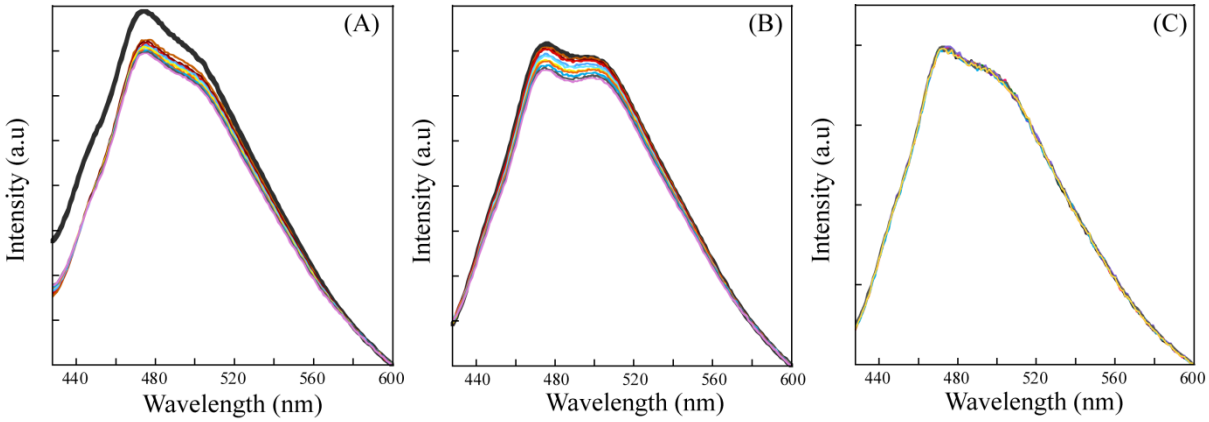

Figure S15: Changes in fluorescence intensity of **L_1-Fe** complex in present of different amounts of proteins. A) metHb B) FBS C)HAS

References:

1. Koch, W.; Holthausen, M. C. *A Chemist's Guide to Density Functional Theory. 2nd edition,* Wiley-VCH, New York, **2000**, 1-300.

2. Gaussian 03, Revision E.01, M. J. Frisch, G. W. Trucks, H. B. Schlegel, G. E. Scuseria, M. A. Robb, J. R. Cheeseman, J. A. Montgomery, Jr., T. Vreven, K. N. Kudin, J. C. Burant, J. M. Millam, S. S. Iyengar, J. Tomasi, V. Barone, B. Mennucci, M. Cossi, G. Scalmani, N. Rega, G. A. Petersson, H. Nakatsuji, M. Hada, M. Ehara, K. Toyota, R. Fukuda, J. Hasegawa, M. Ishida, T. Nakajima, Y. Honda, O. Kitao, H. Nakai, M. Klene, X. Li, J. E. Knox, H. P. Hratchian, J. B. Cross, V. Bakken, C. Adamo, J. Jaramillo, R. Gomperts, R. E. Stratmann, O. Yazyev, A. J. Austin, R. Cammi, C. Pomelli, J. W. Ochterski, P. Y. Ayala, K. Morokuma, G. A. Voth, P. Salvador, J. J. Dannenberg, V. G. Zakrzewski, S. Dapprich, A. D. Daniels, M. C. Strain, O. Farkas, D. K. Malick, A. D. Rabuck, K. Raghavachari, J. B. Foresman, J. V. Ortiz, Q. Cui, A. G. Baboul, S. Clifford, J. Cioslowski, B. B. Stefanov, G. Liu, A. Liashenko, P. Piskorz, I. Komaromi, R. L. Martin, D. J. Fox, T. Keith, M. A. Al-Laham, C. Y. Peng, A. Nanayakkara, M. Challacombe, P. M. W. Gill, B. Johnson, W. Chen, M. W. Wong, C. Gonzalez, and J. A. Pople, Gaussian, Inc., Wallingford CT, 2004.